ACS Energy Letters
http://pubs.acs.org/journal/aelccp

VIEWPOINT

Hidden in Plain Sight: The Overlooked Influence of the Cs^+ Substructure on Transformations in Cesium Lead Halide Nanocrystals

Cite This: ACS Energy Lett. 2020, 5, 3409–3414 Read Online

ACCESS | Metrics & More | Article Recommendations

Cesium lead halide perovskite nanocrystals, with formula $CsPbX_3$ (X = Cl, Br, I), have received enormous attention in the last five years because of their efficient, narrow, and tunable light emission.[1] They crystallize in structures characterized by a three-dimensional network of corner-sharing $[PbX_6]^{4-}$ octahedra (either the perfectly cubic α, or the slightly distorted orthorhombic γ and tetragonal β structures). However, perovskites are only some of the many compositions and structures found in the Cs−Pb−X ternary system: together with the two binary compounds CsX and PbX_2, the best-known structures in the system are Cs_4PbX_6, the perovskites α,β,γ-$CsPbX_3$, the nonperovskite δ-$CsPbX_3$, and $CsPb_2X_5$. The corresponding nanocrystals are highly reactive systems that can readily undergo chemical and structural transformations in response to changes in their surroundings.[1,2] Rationalizing the reactivity of these materials is crucial for two reasons. First, for their stabilization. Second, to create opportunities for processability and applications.

The reports describing compositional and structural interconversions are often focused on pairs of compounds, e.g., the $CsPbX_3 \rightleftarrows Cs_4PbX_6$ or the $CsPbX_3 \rightleftarrows Cs_4Pb_2X_5$. However, as more experimental data have become available over time, it is now possible to connect different reactions and construct a unifying picture of the reactivity of the Cs−Pb−X compounds. Such a view has been missing to date, mainly because these materials are often approached with a focus on how their structures are related to their properties and less to their reactivity. In fact, $[PbX_6]^{4-}$ octahedra are usually considered as the main structural motif in lead halide perovskite and perovskite-related structures. Such octahedra are disconnected in Cs_4PbX_6, but share corners in the perovskite $CsPbX_3$ and faces in the δ-$CsPbX_3$ nonperovskite structure. This rationalization is useful when discussing electronic properties, as they mostly depend on the Pb−X−Pb connectivity.[3] However, reasoning in terms of $[PbX_6]^{4-}$ octahedra excludes many of the materials in the Cs−Pb−X system that can either generate or be generated from one of the three above through a chemical reaction and hides deeper structural connections across the whole series. For example, CsX nanocrystals can be transformed into $CsPbX_3$ nanocrystals,[4] and $CsPb_2X_5$ can be obtained by thermal decomposition of $CsPbX_3$ nanocrystals.[5] Neither CsX nor $CsPb_2X_5$ actually contains $[PbX_6]^{4-}$ octahedra: lead in $CsPb_2X_5$ features an unusual $[PbX_8]^{6-}$ biaugmented triangular prism octa-coordination.[6]

In this Viewpoint, we present a different way of approaching this whole set of compounds. Instead of $[PbX_6]^{4-}$ octahedra, we take the arrangement of Cs^+ cations as the leading structural motif (Figure 1). From such a perspective, the

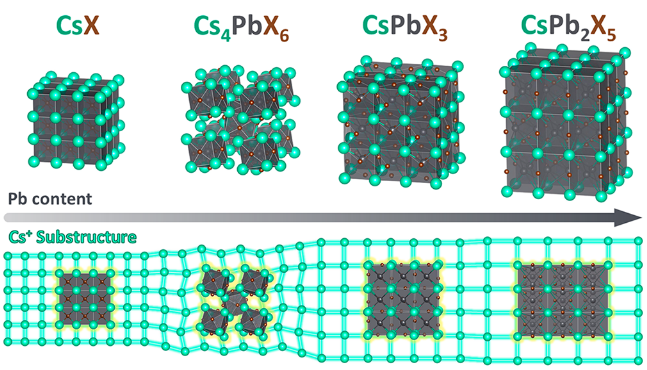

Figure 1. Crystal structures of CsX, Cs_4PbX_6, $CsPbX_3$, and $CsPb_2X_5$ compounds shown in order of increasing lead content (top panel) and interconnected by a common structural motif: a substructure of Cs^+ cations that expands and distorts along with the series (bottom panel).

parent structure of the group is CsX, where the Cs^+ ions form a substructure of cubic cages, each enclosing a single halide ion. Such a substructure is found in all the other compounds (except for δ-$CsPbX_3$), albeit expanded and sometimes distorted. Starting from the parent structure CsX, we can replace X^- ions with composite $[Pb_nX_{2n+1}]^-$ polyanions, which

Received: September 22, 2020
Accepted: October 1, 2020

   https://dx.doi.org/10.1021/acsenergylett.0c02029
ACS Energy Lett. 2020, 5, 3409−3414

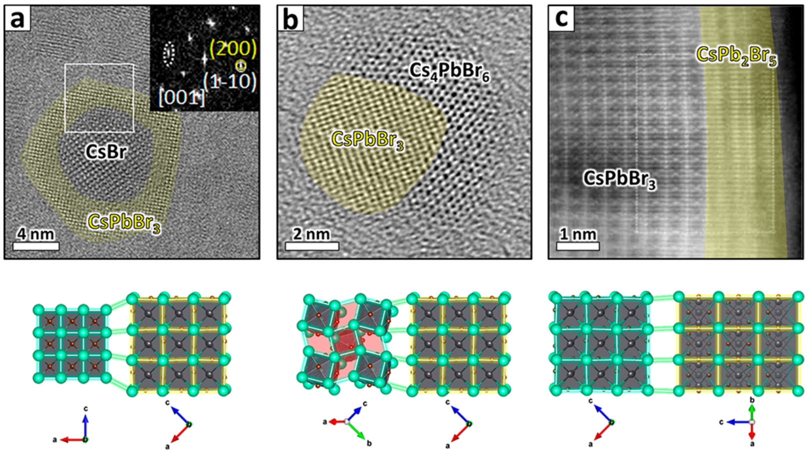

Figure 2. Epitaxial heterostructures between pairs of Cs−Pb−Br compounds. From left to right: high-resolution TEM images of CsBr-$CsPbBr_3$, Cs_4PbBr_6−$CsPbBr_3$ and $CsPbBr_3$−$CsPb_2Br_5$, heterostructures.[4,7,8] The bottom sketches are simplified models of the epitaxial connections, highlighting the expansion and distortion of the Cs^+ substructure when moving from lead-poor to lead-rich compounds. The lead-rich compounds are shaded in yellow, and the empty cages in the Cs_4PbBr_6 structure are shaded in red. Crystallographic axes are shown to clarify the relative orientation of the crystal structures. The HRTEM image in panel a is reproduced from ref 7; those in panels b and c are reproduced from refs 4 and 8 with permission from the Royal Society of Chemistry and Springer Nature, respectively.

is equivalent to adding n units of PbX_2 to each unit of CsX. Depending on the amount of PbX_2 added, the anionic network adapts its connectivity to ensure the charge balance, and we obtain the whole series of structures.

We begin with Cs_4PbX_6, where only one-fourth of the Cs^+ cages incorporate lead in the form of disconnected $[PbX_6]^{4-}$ ions, resulting in an average $[Pb_{0.25}X_{1.5}]^-$ polyanion per cage. Note that the filled cages retain a cubic shape, while the empty ones distort to become rhombohedral (Figure 2, the empty cages in the Cs_4PbBr_6 structure are shaded in red). That distortion makes the Cs^+ cations in the corner of one cube interact with X^- anions on the faces of the surrounding cubes and produces an overall change in symmetry from cubic to hexagonal. In $CsPbX_3$, all the cages become filled with $[PbX_3]^-$. In each cage, the center is taken by Pb^{2+} ions, while X^- ions are on the faces, shared between neighboring cages. This is equivalent to the more familiar description of the structure through corner-sharing $[PbX_6]^{4-}$ octahedra. Moving along the series, in $CsPb_2X_5$, each cage encloses a $[Pb_2X_5]^-$ polyanion. Here, the two Pb^{2+} cations and four of the five X^- anions are inside the cage, while the remaining X^- anion is found at one edge and is therefore shared with the neighboring cages. This configuration leads to a connected network of $[PbX_8]^{6-}$ biaugmented triangular prisms. $PbBr_2$, which has no Cs^+ substructure, should not be considered as next in the list. However, it is interesting to notice that the Pb^{2+} ions in it share the same coordination found in $CsPb_2X_5$, although the connectivity changes to keep the structure charge-balanced. In this sense, PbX_2 can be imagined as an infinitely large $[Pb_nX_{2n+1}]^-$ network (with $n \to \infty$) enclosed in a Cs^+ cage where the Cs−Cs distance has expanded to infinity.

The existence of a common structural motif helps to explain the reactivity of cesium lead halide compounds: in essence, the preservation of the Cs^+ substructure allows the transformation to take place without tearing the whole crystal structure apart. In our discussion, we will be focusing mainly on the Cs−Pb−Br system, because the many reports on these materials provide enough experimental data to test our mechanistic hypothesis. Especially, we will refer to nanocrystals since they are ideal systems to study transformations because of their fast reaction kinetics and the possibility of direct observations with transmission electron microscopy (TEM). However, the structural relationships between compounds exist regardless of the crystal size, thus it applies to bulk materials as well.

The simplest structure in the series is CsBr. Shamsi et al. achieved the transformation of CsBr nanocrystals to γ-$CsPbBr_3$ perovskite nanocrystals by reaction with $Pb(oleate)_2$.[4] The transformation preserved the nanocrystal size distribution, pointing against a complete dissolution−recrystallization mechanism (i.e., in which all CsBr is dissolved and $CsPbBr_3$ is nucleated from free ions in solution). Instead, the reaction proceeded by the progressive insertion of $PbBr_2$ into the CsBr structure, with Pb^{2+} coming from $Pb(oleate)_2$ and Br^- from a partial etching of the nanocrystal surface. The reported observation of intermediate CsBr@$CsPbBr_3$ core−shell epitaxial heterostructures supports our proposed mechanism (Figure 2a). The average size of the heterostructures became smaller as the transformation proceeded, accounting for the partial surface etching and the release of excess Cs^+ in the environment. At the same time, the epitaxial connection ensured that the Cs^+ substructure was shared between the two domains. As expected, the large difference of crystal structure constants (CsBr = 4.3 Å; $CsPbBr_3$ = 5.8 Å) produced strain at the interface, which was measured by high-resolution TEM.

The next and much more extensively studied set of transformations concerns the conversion of $CsPbBr_3$ to Cs_4PbBr_6 and back. This equilibrium was reported to be reversible and easily triggerable by a variety of stimuli: addition and subtraction of $PbBr_2$ or CsBr and changes in the concentration of ligands in the environment. One interesting example was reported by Li et al., who cycled the transformation back and forth while retaining the nanocrystal size distribution.[9] Specifically, the $CsPbBr_3 \to Cs_4PbBr_6$ reaction was triggered by adding a mixture of ligands (oleic acid and oleylamine), which increased the $PbBr_2$ solubility in the environment, while the inverse $Cs_4PbBr_6 \to CsPbBr_3$ reaction was driven by the direct addition of $PbBr_2$. Remarkably, they observed that the nanocrystal size at each cycle of the transformation was compatible with a constant number of Cs^+

atoms. All these observations are consistent with a substructure-preserving reaction mechanism: $PbBr_2$ is readily incorporated in (or released by) each Cs^+ cage, as the process requires only a mild distortion of the Cs^+ substructure. Baranov et al. provided a strong proof for this mechanism: while studying the $Cs_4PbBr_6 \rightarrow CsPbBr_3$ transformation, they isolated intermediate $CsPbBr_3$−Cs_4PbBr_6 epitaxial heterostructures where the Cs^+ substructure was continuous across the whole nanocrystals, with little distortion at the interfacial regions (Figure 2b).[7] Interestingly, the transformation proceeded from one single nucleation point on the nanocrystal surface, and from there it extended to the remaining regions. The absence of multiple nucleation points of the $CsPbBr_3$ phase on a single nanocrystal can be explained based on the proposed mechanism: once the transformation is started, the strain induced by the epitaxial connection locally straightens the distorted Cs^+ substructure of Cs_4PbBr_6 to match that of $CsPbBr_3$. This local expansion facilitates the further diffusion of $PbBr_2$ at the domain interface, resulting in a sort of self-catalyzed reaction.

Another interesting example is the $Cs_4PbBr_6 \rightarrow CsPbBr_3$ transformation driven by CsBr extraction. This was reported upon the reaction of nanocrystals with solid Prussian Blue ($Fe^{III}{}_4[Fe^{II}(CN)_6]_3$),[10] which is known to selectively intercalate Cs^+, or after their exposure to a hexane−water interface.[11] In both cases, no intermediate heterostructures were isolated, although the size distribution of the nanocrystals was preserved, evidence that again played against a dissolution−recrystallization mechanism. Also, the nanocrystals contracted in size after the reaction, as expected from a partial etching. This is a key point to rationalize the observations based on our proposed transformation mechanism. Cs_4PbBr_6 nanocrystals indeed should undergo etching when CsBr is extracted from their surface. However, for each four CsBr units etched away, one unit of $PbBr_2$ is also freed. No $PbBr_2$ was detected at the end of the process by XRD, and that can be explained by $PbBr_2$ re-entering the remaining portion of the Cs_4PbBr_6 nanocrystals, driving the transformation to $CsPbBr_3$ nanocrystals. The extraction of Cs^+ ions stopped when what remained of the etched nanocrystals had been entirely converted to $CsPbBr_3$: any further extraction of CsBr would have been accompanied by the extraction of $PbBr_2$, which, as already said, was not detected in the final product. Furthermore, Wu et al. compared the volume of particles before and after the water-driven transformation, finding it compatible with a constant number of Pb atoms (Cs_4PbBr_6 diameter = 17.8 nm; $CsPbBr_3$ expected/measured = 10.8/12.2 nm).[11] We repeated the analysis for the Prussian Blue driven transformation, finding an excellent match (Cs_4PbBr_6 diameter = 9.8 nm; $CsPbBr_3$ expected/measured = 5.9/6.3 nm). This further supports our mechanistic hypothesis. It is worth mentioning that a dissolution−recrystallization mechanism in these types of reactions is still possible, given the right conditions. For example, Palazon et al. and Udayabhaskararao et al. both triggered the $CsPbX_3 \rightarrow Cs_4PbX_6$ transformation by adding amines, which can sequestrate lead by forming a complex.[12,13] However, ammonium ions are known to compete with Cs^+ ions in the lead halide perovskite structure, thus causing the Cs^+ substructure degradation and the consequent recrystallization.[14,15]

To conclude the series, fewer reports exist on the $CsPbBr_3 \rightarrow CsPb_2Br_5$ transformation, mainly because of the less appealing optical and electronic properties of $CsPb_2Br_5$. In general, this transformation is slower than the previous ones or requires harsher conditions such as continuous illumination or heating.[2,16] For example, Huang *et al.* reacted $CsPbBr_3$ nanosheets with an excess of $PbBr_2$ at 60 °C for 3 days, obtaining epitaxial heterostructures.[17] Because there is little interest in pure $CsPb_2Br_5$, the transformation was halted at that stage. The preservation of the Cs^+ substructure helps to rationalize these observations as well. The $CsPbBr_3 \rightarrow CsPb_2Br_5$ transformation stretches the Cs^+ cages in one direction, lowering their symmetry from cubic to tetragonal. As a consequence, the crystal structure parameter in the elongated direction becomes too large (9.7 Å) to match with that of $CsPbBr_3$, leaving only the (001) plane as a possible interface between $CsPbBr_3$ and $CsPb_2Br_5$. The high-quality HRTEM images captured by Zheng et al. on a cosynthesized heterostructure help to visualize this connection (Figure 2c).[8] The main consequence of this structural constraint is that the transformation cannot proceed cell-by-cell as for the previous examples: it must take place layer by layer, largely increasing the required activation energy and slowing down the reaction.

Overall, the preservation of the Cs^+ substructure weaves a thread connecting the various reactions in the Cs−Pb−X system. Its main merit is to outline a common reaction mechanism, based on the intercalation/extraction of $PbBr_2$ from lead-poor/rich compounds, which proceeds via epitaxial heterostructures and preserves the nanocrystal size and size distribution. In this sense, trying to predict or model the response of the Cs^+ substructure to transformations can offer new insights into those reactions that we expect to occur but have not been observed to date. For example, the $CsBr \rightarrow CsPbBr_3$ transformation seems to bypass the anticipated Cs_4PbBr_6 intermediate. The reason is likely found in the self-catalyzed $Cs_4PbBr_6 \rightarrow CsPbBr_3$ transformation discussed above: Cs_4PbBr_6 might form in the early stages of the reaction, but the incoming $PbBr_2$ will likely react more favorably with it, forming $CsPbBr_3$, than with CsBr. Yet, small domains of Cs_4PbBr_6, although not observed to date, may exist at the $CsBr$−$CsPbBr_3$ interface, acting as a strain-releasing transient layer.

Moving to other halides, an interesting observation is that both CsI and Cs_4PbI_6 nanocrystals react with $Pb(oleate)_2$ and PbI_2, respectively, forming the metastable but desirable black $CsPbI_3$ perovskite phase instead of the thermodynamically favored wide-gap δ-$CsPbI_3$.[4,18] The preservation of the Cs^+ substructure helps to rationalize that reaction route. The arrangement of Cs^+ ions in δ-$CsPbI_3$ is completely different from that found in CsI and Cs_4PbI_6; thus, the transformation from CsI or Cs_4PbI_6 to δ-$CsPbI_3$ would require a major structural rearrangement of the Cs^+ substructure and hence high activation energy. Instead, both CsI and Cs_4PbI_6 transform to the more structurally compatible $CsPbI_3$ perovskite structure, both transformations requiring much lower activation energy. In nanocrystals, the perovskite $CsPbI_3 \rightarrow \delta$-$CsPbI_3$ transformation slowly happens soon after, likely by a recrystallization mechanism, posing a challenge to the applications of this promising material, for example, in solar cells.[19,20]

Another example of a process preserving the Cs^+ substructure is the γ-$CsPbBr_3 \rightarrow \gamma$-$CsPbI_3$ halide-exchange reaction.[21,22] The reverse transformation in bulk compounds has been recently reported for the nonperovskite phases, δ-$CsPbI_3 \rightarrow \delta$-$CsPbBr_3$.[23] These two reactions involve

https://dx.doi.org/10.1021/acsenergylett.0c02029
ACS Energy Lett. 2020, 5, 3409−3414

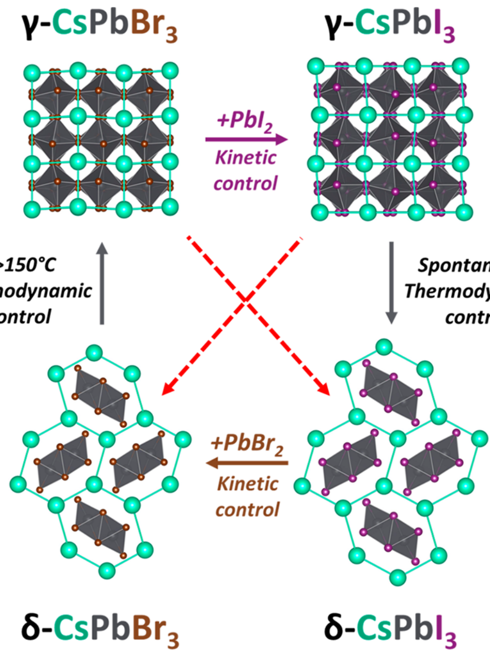

Figure 3. Summary of the transformations between the γ-perovskite and δ-nonperovskite polymorphs of $CsPbBr_3$ and $CsPbI_3$. Ion-exchange reactions (indicated by purple and brown arrows) that preserve the Cs^+ substructure are under kinetic control and produce metastable structures. Instead, the thermodynamically favored structures are generated by reactions (indicated by red dashed arrows) that do not preserve the Cs^+ substructure. The metastable structures convert to the stable ones either spontaneously in nanocrystals ($CsPbI_3$) or upon heating in bulk powders ($CsPbBr_3$).

completely different structures yet share similarities (Figure 3). Both transform a stable structure (γ-$CsPbBr_3$ or δ-$CsPbI_3$) into a metastable one (γ-$CsPbI_3$ or δ-$CsPbBr_3$, respectively) under kinetic control, and both preserve the Cs^+ substructure. The Cs^+ substructure acts as a backbone in both γ and δ structures (the arrangement of $[PbX_6]^{4-}$ octahedra is preserved as well) during anion exchange. The further transformation to the stable γ-$CsPbBr_3$ phase could be achieved only by raising the temperature above 150 °C, indicating the high activation energy required to disrupt and rearrange the Cs^+ substructure.

The last case we discuss is that of Cs_2PbX_4. This stoichiometry is intermediate between Cs_4PbX_6 and $CsPbX_3$, corresponds to Cs^+ cages filled with $[Pb_{0.5}X_2]^-$ anions on average, and exists in the form of the Ruddlesden−Popper $Cs_2PbCl_2I_2$ structure (Figure 4, middle model).[24] Here, the difference in size between Cl^- and I^- helps to stabilize the structure. The $Cs_2PbCl_2I_2$ structure features cubic Cs^+ cages filled with $[PbCl_2I_2]^{2-}$ alternated with distorted noncubic empty cages, for an average $[Pb_{0.5}ClI]^-$ unit per cage, and hence fits into the structural series discussed so far. The filled cages are shifted by half-cell to let Cs^+ in one layer interact with I^- in the neighboring one and provide a stabilizing interaction for the structure, similarly to Cs_4PbX_6. Reactions involving Ruddlesden−Popper metal halide nanocrystals are rare; however, a recent work reported the transformation of $Cs_2PbCl_2I_2$ nanoplates into nanocrystals of γ-$CsPbBr_3$ and Cs_4PbCl_6 by reaction with $PbBr_2$ and $MnCl_2$, respectively.[25] Although there is not sufficient data to exclude recrystallization, it is worth pointing out that the Cs^+ substructure in $Cs_2PbCl_2I_2$ can be derived from that of γ-$CsPbX_3$ by

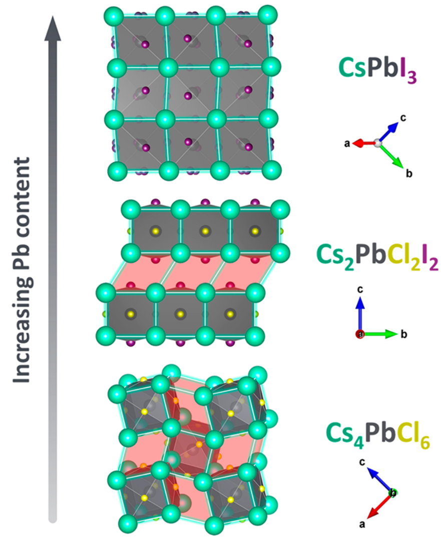

Figure 4. Ruddlesden−Popper metal halide $Cs_2PbCl_2I_2$ (middle) has an intermediate structure between that of lead-rich $CsPbI_3$ (top) and the lead-poor Cs_4PbCl_6 (bottom), into which it can be transformed. The three structures share similarities in the cubic Cs^+ substructures, albeit with different numbers of cubic cages filled by lead halide polyanions. Empty cages in the front layer are highlighted in red. Crystallographic axes are shown to clarify the relative orientation of the Cs^+ substructure and the unit cell.

alternating distortions of one layer of cages (the empty ones) while leaving the other layer almost intact (the filled ones).

The outcomes of the $Cs_2PbCl_2I_2$ reactions with $PbBr_2$ and $MnCl_2$ can be explained through the principle of Cs^+ substructure preservation. The addition of $MnCl_2$ would cause an I → Cl halide exchange to a hypothetical Cs_2PbCl_4 structure that is not stable and must decompose. In parallel, Mn^{2+} is not able to replace Pb^{2+} in $CsPbCl_3$ in large amounts,[26] leaving the material the only option of expelling PbI_2 and converting into stable Cs_4PbCl_6. From the Cs^+ substructure point of view, this requires tilting of the cages, as half of them become empty. Instead, the addition of $PbBr_2$ proceeds with the replacement of both I^- and Cl^- by an intermediate-sized Br^- along with further incorporation of $PbBr_2$, which removes the distortions of the Cs^+ substructure and delivers a stable γ-$CsPbBr_3$. Such analysis yields a prediction that lead halide nanocrystals of Ruddlesden−Popper compounds could be obtained from Cs_4PbX_6 by PbX_2 insertion. That line of thinking opens a perspective onto Cs_4PbX_6 nanocrystals as precursors for multinary metal halide nanocrystals through the reactive intercalation of PbX_2 and other metal halide M_nX_m species.

To conclude, the discussed preservation of the Cs^+ substructure could be an example of the general "A" cation substructure preservation applicable to other halides. For example, compounds where Cs^+ is replaced by organic cations such as methylammonium or formamidinium often crystallize in analogous structures (e.g., α,β,γ-$MAPbX_3$ and MA_4PbX_6,[27,28] where MA = methylammonium). Studies on their reactivity are highly focused on the substructure-destructive γ-$MAPbI_3$ → δ-$MAPbI_3$ transformation that poses huge challenges to the development of perovskite-based photovoltaics.[29] However, we expect organic cation-based halides to show substructure-conservative transforma-

https://dx.doi.org/10.1021/acsenergylett.0c02029
ACS Energy Lett. 2020, 5, 3409−3414

tions like those of cesium compounds. The "A" cation substructure preservation is also expected to hold in structures where the B cation is different from Pb^{2+}, such as Sn^{2+} or Ge^{2+}. Further on, it will be interesting to explore if a similar principle applies to more complex structures such as the double perovskites, where the pairs of Pb^{2+} cations of $CsPbX_3$ are replaced by B^+ and B'^{3+} cations, opening up to investigation a vastly untapped array of possible transformations.

Stefano Toso
Dmitry Baranov orcid.org/0000-0001-6439-8132
Liberato Manna orcid.org/0000-0003-4386-7985

AUTHOR INFORMATION

Complete contact information is available at:
https://pubs.acs.org/10.1021/acsenergylett.0c02029

Notes

Views expressed in this Viewpoint are those of the authors and not necessarily the views of the ACS.
The authors declare no competing financial interest.

ACKNOWLEDGMENTS

We thank Dr. Francisco Palazon and Dr. Javad Shamsi for helpful discussions.

REFERENCES

(1) Yang, D.; Cao, M.; Zhong, Q.; Li, P.; Zhang, X.; Zhang, Q. All-Inorganic Cesium Lead Halide Perovskite Nanocrystals: Synthesis, Surface Engineering and Applications. *J. Mater. Chem. C* **2019**, *7*, 757−789.
(2) Li, J.; Zhang, H.; Wang, S.; Long, D.; Li, M.; Wang, D.; Zhang, T. Inter-Conversion between Different Compounds of Ternary Cs-Pb-Br System. *Materials* **2018**, *11* (5), 717.
(3) Quarti, C.; Katan, C.; Even, J. Physical Properties of Bulk, Defective, 2D and 0D Metal Halide Perovskite Semiconductors from a Symmetry Perspective. *JPhys Mater.* **2020**, *3* (4), 042001.
(4) Shamsi, J.; Dang, Z.; Ijaz, P.; Abdelhady, A. L.; Bertoni, G.; Moreels, I.; Manna, L. Colloidal CsX (X = Cl, Br, I) Nanocrystals and Their Transformation to $CsPbX_3$ Nanocrystals by Cation Exchange. *Chem. Mater.* **2018**, *30* (1), 79−83.
(5) Palazon, F.; Dogan, S.; Marras, S.; Locardi, F.; Nelli, I.; Rastogi, P.; Ferretti, M.; Prato, M.; Krahne, R.; Manna, L. From $CsPbBr_3$ Nano-Inks to Sintered $CsPbBr_3$-$CsPb_2Br_5$ Films via Thermal Annealing: Implications on Optoelectronic Properties. *J. Phys. Chem. C* **2017**, *121* (21), 11956−11961.
(6) Li, G.; Wang, H.; Zhu, Z.; Chang, Y.; Zhang, T.; Song, Z.; Jiang, Y. Shape and Phase Evolution from $CsPbBr_3$ Perovskite Nanocubes to Tetragonal $CsPb_2Br_5$ Nanosheets with an Indirect Bandgap. *Chem. Commun.* **2016**, *52* (75), 11296−11299.
(7) Baranov, D.; Caputo, G.; Goldoni, L.; Dang, Z.; Scarfiello, R.; De Trizio, L.; Portone, A.; Fabbri, F.; Camposeo, A.; Pisignano, D.; et al. Transforming Colloidal Cs_4PbBr_6 Nanocrystals with Poly(maleic anhydride-alt−1-octadecene) into Stable $CsPbBr_3$ Perovskite Emitters through Intermediate Heterostructures. *Chem. Sci.* **2020**, *11* (15), 3986−3995.
(8) Zheng, Y.; Yang, T.; Fang, Z.; Shang, M.; Zhang, Z.; Yang, J.; Fan, J.; Yang, W.; Hou, X.; Wu, T. All-Inorganic Dual-Phase Halide Perovskite Nanorings. *Nano Res.* **2020**, *13* (11), 2994−3000.
(9) Li, Y.; Huang, H.; Xiong, Y.; Kershaw, S. V.; Rogach, A. L. Reversible Transformation between $CsPbBr_3$ and Cs_4PbBr_6 Nanocrystals. *CrystEngComm* **2018**, *20* (34), 4900−4904.
(10) Palazon, F.; Urso, C.; De Trizio, L.; Akkerman, Q.; Marras, S.; Locardi, F.; Nelli, I.; Ferretti, M.; Prato, M.; Manna, L. Postsynthesis Transformation of Insulating Cs_4PbBr_6 Nanocrystals into Bright Perovskite $CsPbBr_3$ through Physical and Chemical Extraction of CsBr. *ACS Energy Lett.* **2017**, *2* (10), 2445−2448.
(11) Wu, L.; Hu, H.; Xu, Y.; Jiang, S.; Chen, M.; Zhong, Q.; Yang, D.; Liu, Q.; Zhao, Y.; Sun, B.; et al. From Nonluminescent Cs_4PbX_6 (X = Cl, Br, I) Nanocrystals to Highly Luminescent $CsPbX_3$ Nanocrystals: Water-Triggered Transformation through a CsX-Stripping Mechanism. *Nano Lett.* **2017**, *17* (9), 5799−5804.
(12) Palazon, F.; Almeida, G.; Akkerman, Q. A.; De Trizio, L.; Dang, Z.; Prato, M.; Manna, L. Changing the Dimensionality of Cesium Lead Bromide Nanocrystals by Reversible Postsynthesis Transformations with Amines. *Chem. Mater.* **2017**, *29* (10), 4167−4171.
(13) Udayabhaskararao, T.; Houben, L.; Cohen, H.; Menahem, M.; Pinkas, I.; Avram, L.; Wolf, T.; Teitelboim, A.; Leskes, M.; Yaffe, O.; et al. A Mechanistic Study of Phase Transformation in Perovskite Nanocrystals Driven by Ligand Passivation. *Chem. Mater.* **2018**, *30* (1), 84−93.
(14) Almeida, G.; Infante, I.; Manna, L. Resurfacing Halide Perovskite Nanocrystals. *Science* **2019**, *364*, 833−834.
(15) Quarta, D.; Imran, M.; Capodilupo, A. L.; Petralanda, U.; Van Beek, B.; De Angelis, F.; Manna, L.; Infante, I.; De Trizio, L.; Giansante, C. Stable Ligand Coordination at the Surface of Colloidal $CsPbBr_3$ Nanocrystals. *J. Phys. Chem. Lett.* **2019**, *10* (13), 3715−3726.
(16) Shen, W.; Ruan, L.; Shen, Z.; Deng, Z. Reversible Light-Mediated Compositional and Structural Transitions between $CsPbBr_3$ and $CsPb_2Br_5$ Nanosheets. *Chem. Commun.* **2018**, *54* (22), 2804−2807.
(17) Huang, Z. P.; Ma, B.; Wang, H.; Li, N.; Liu, R. T.; Zhang, Z. Q.; Zhang, X. D.; Zhao, J. H.; Zheng, P. Z.; Wang, Q.; et al. In Situ Growth of 3D/2D ($CsPbBr_3$/$CsPb_2Br_5$) Perovskite Heterojunctions toward Optoelectronic Devices. *J. Phys. Chem. Lett.* **2020**, *11* (15), 6007−6015.
(18) Akkerman, Q. A.; Park, S.; Radicchi, E.; Nunzi, F.; Mosconi, E.; De Angelis, F.; Brescia, R.; Rastogi, P.; Prato, M.; Manna, L. Nearly Monodisperse Insulator Cs_4PbX_6(X = Cl, Br, I) Nanocrystals, Their Mixed Halide Compositions, and Their Transformation into $CsPbX_3$ Nanocrystals. *Nano Lett.* **2017**, *17* (3), 1924−1930.
(19) Straus, D. B.; Guo, S.; Cava, R. J. Kinetically Stable Single Crystals of Perovskite-Phase $CsPbI_3$. *J. Am. Chem. Soc.* **2019**, *141* (29), 11435−11439.
(20) Swarnkar, A.; Marshall, A. R.; Sanehira, E. M.; Chernomordik, B. D.; Moore, D. T.; Christians, J. A.; Chakrabarti, T.; Luther, J. M. Quantum Dot-Induced Phase Stabilization of α-$CsPbI_3$ Perovskite for High-Efficiency Photovoltaics. *Science* **2016**, *354* (6308), 92−95.
(21) Nedelcu, G.; Protesescu, L.; Yakunin, S.; Bodnarchuk, M. I.; Grotevent, M. J.; Kovalenko, M. V. Fast Anion-Exchange in Highly Luminescent Nanocrystals of Cesium Lead Halide Perovskites ($CsPbX_3$, X = Cl, Br, I). *Nano Lett.* **2015**, *15* (8), 5635−5640.
(22) Akkerman, Q. A.; D'Innocenzo, V.; Accornero, S.; Scarpellini, A.; Petrozza, A.; Prato, M.; Manna, L. Tuning the Optical Properties of Cesium Lead Halide Perovskite Nanocrystals by Anion Exchange Reactions. *J. Am. Chem. Soc.* **2015**, *137* (32), 10276−10281.
(23) Aebli, M.; Benin, B. M.; McCall, K. M.; Morad, V.; Thöny, D.; Grützmacher, H.; Kovalenko, M. V. White $CsPbBr_3$: Characterizing the One-Dimensional Cesium Lead Bromide Polymorph. *Helv. Chim. Acta* **2020**, *103* (7), e2000080.
(24) Akkerman, Q. A.; Bladt, E.; Petralanda, U.; Dang, Z.; Sartori, E.; Baranov, D.; Abdelhady, A. L.; Infante, I.; Bals, S.; Manna, L. Fully Inorganic Ruddlesden-Popper Double Cl-I and Triple Cl-Br-I Lead Halide Perovskite Nanocrystals. *Chem. Mater.* **2019**, *31* (6), 2182−2190.
(25) Acharyya, P.; Maji, K.; Kundu, K.; Biswas, K. 2D Nanoplates and Scaled-Up Bulk Polycrystals of Ruddlesden-Popper $Cs_2PbI_2Cl_2$ for Optoelectronic Applications. *ACS Appl. Nano Mater.* **2020**, *3* (1), 877−886.
(26) Parobek, D.; Dong, Y.; Qiao, T.; Son, D. H. Direct Hot-Injection Synthesis of Mn-Doped $CsPbBr_3$ Nanocrystals. *Chem. Mater.* **2018**, *30* (9), 2939−2944.
(27) Ju, M. G.; Dai, J.; Ma, L.; Zhou, Y.; Zeng, X. C. Zero-Dimensional Organic-Inorganic Perovskite Variant: Transition between Molecular and Solid Crystal. *J. Am. Chem. Soc.* **2018**, *140* (33), 10456−10463.

(28) Brivio, F.; Frost, J. M.; Skelton, J. M.; Jackson, A. J.; Weber, O. J.; Weller, M. T.; Goñi, A. R.; Leguy, A. M. A.; Barnes, P. R. F.; Walsh, A. Lattice Dynamics and Vibrational Spectra of the Orthorhombic, Tetragonal, and Cubic Phases of Methylammonium Lead Iodide. *Phys. Rev. B* **2015**, *92* (14), 144308.

(29) Zhang, Y.; Zhou, Z.; Ji, F.; Li, Z.; Cui, G.; Gao, P.; Oveisi, E.; Nazeeruddin, M. K.; Pang, S. Trash into Treasure: δ-$FAPbI_3$ Polymorph Stabilized $MAPbI_3$ Perovskite with Power Conversion Efficiency beyond 21%. *Adv. Mater.* **2018**, *30* (22), 1707143.

https://dx.doi.org/10.1021/acsenergylett.0c02029
ACS Energy Lett. 2020, 5, 3409−3414